Mean and Turbulent Structures of the Oceanic Surface Layer as Determined from One-Dimensional, Third-Order Simulations

JEAN CLAUDE ANDRÉ* AND PIERRE LACARRÈRE

Centre National de Recherches Météorologiques (DMN/EERM), 31057 Toulouse Cedex, France

(Manuscript received 15 June 1982, in final form 17 September 1984)

ABSTRACT

Various mechanisms that can drive the evolution of the oceanic surface boundary layer (OSBL) are numerically studied using a detailed turbulence-closure scheme. It is shown that stress- and shear-driven regions are characterized by relatively poor mixing of momentum and heat, and by a local equilibrium at each level between shear production and destruction by viscous dissipation and buoyancy. Buoyancy-driven regions appear to be much more well mixed and to be characterized by counter-gradient turbulent diffusion of eddy kinetic energy. Consequences of these features for the parameterization and description of the OSBL are discussed.

1. Introduction and motivations

Since the early work of Kraus and Turner (1967), a number of models have been applied to the numerical simulation of the oceanic surface boundary layer (OSBL). One can distinguish between three main approaches. On the one hand, many models deal only with bulk, or integral, properties of the OSBL, like the ones developed by Denman and Miyake (1973), Lacombe (1974), Thompson (1976), Garwood (1977) or Posmentier (1980). In such models it is usually assumed that turbulence is efficient enough to completely mix momentum, heat and salt in the OSBL. In the second kind of approach, the vertical structure of the OSBL is explicitly resolved by using multi-layered numerical models where turbulence is taken into account through more or less sophisticated schemes. The first model of this kind, to the author's knowledge, has been implemented by Mellor and Durbin (1975) who used a Richardson-number dependent eddy-diffusivity coefficient. Further improvements were proposed by Svensson (1979), Warn-Varnas and Piacsek (1979)[1], Kundu (1980a), and Klein and Coantic (1981). These various models do not agree on one point, as clearly stated in the correspondence between Deardorff (1980) and Kundu (1980b): what is the relative importance of downward turbulent propagation of eddy kinetic energy with respect to erosion of the thermocline? In other words, it is not clearly known if triple-correlation terms (like the turbulent kinetic energy flux $w'e = \frac{1}{2}w'(u'^2 + v'^2 + w'^2)$) have to be carefully parameterized or not in such models. A second question that arises when one considers the results obtained from these one-dimensional (1-d) models concerns the validity of the mixed-layer assumption used in most integral models of the first kind. Almost all of the 1-d models exhibit indeed a vertical structure with significant gradients, at least with significant shear. This probably led some authors to give up with the well-mixed assumption and to describe the vertical profiles by using instead a self-similarity approach (e.g., see Mellor and Strub, 1980; Kundu, 1981; Cushman-Roisin, 1982). This point is of physical interest since it has been recently shown (André *et al.*, 1979b; Mahrt and André, 1983) that significant vertical gradients may survive in turbulent boundary layers entraining rapidly layers of quiescent fluid with different properties.

In the present paper one proposes to use a fairly detailed turbulence model to look for answers to the already mentioned questions:

(i) Is the vertical turbulent diffusion efficient enough to export any noticeable amount of eddy kinetic energy down to the interface with the thermocline and to erode it?

(ii) Are current and temperature well mixed in a thickening OSBL or, equivalently, which kind of vertical profile must be used when developing bulk models for the OSBL?

These two questions are very difficult to answer from examination of real-world data. Current profile measurements are indeed very rare (nevertheless, see

* Part of the work was done while this author was visiting the Department of Atmospheric Sciences at Oregon State University (August 1980–February 1981).

[1] There is a difficulty in understanding Warn-Varnas and Piacsek's results. They indeed show (their Fig. 5) an eddy kinetic energy budget where the shear production is a sink term for eddy kinetic energy.

Chouchan, 1981; Price *et al.*, 1984, for examples of poor momentum mixing in the OSBL) and it is furthermore almost impossible to document experimentally the budget of turbulent kinetic energy at the interface between the OSBL and the thermocline.

The only feasible alternative appears then to use a numerical model. Such a model must of course be sufficiently sophisticated that one is reasonably sure it includes most of the turbulent processes that are thought to be of importance. It is also necessary that it has been carefully tested before, against many experimentally documented cases. In addition to the fact they allow for a better understanding of the dynamics of turbulent OSBL, such model simulations may also be used to calibrate simpler parameterized models. This has been done for both cases of atmospheric boundary layer (Therry and Lacarrère, 1983) and OSBL (Gaspar, 1984). The model used here is the third-order closure scheme of André *et al.* (1976a), previously developed for the study of the atmospheric planetary boundary layer (André *et al.*, 1978) and tested against laboratory experiments on shear- and buoyancy-driven turbulence (André *et al.*, 1979a; André *et al.*, 1982).

2. The numerical model

The numerical model used in the present study is based on the Boussinesq approximation and on the horizontal homogeneity assumption. In such a simplified case it is possible simply to deal with two mean parameters, the current velocity $\bar{u}$ and temperature $\bar{T}$, whose rate equations can be written as

$$\frac{\partial \bar{u}}{\partial t} = -\frac{\partial \overline{u'w'}}{\partial z}, \tag{1}$$

$$\frac{\partial \bar{T}}{\partial t} = -\frac{\partial \overline{w'T'}}{\partial z}. \tag{2}$$

The calculation of the vertical turbulent fluxes of momentum and heat requires the knowledge of other fluxes and variances, that is we deal with six double correlations: the horizontal and vertical heat fluxes $\overline{u'T'}$ and $\overline{w'T'}$, the momentum flux $\overline{u'w'}$, the eddy kinetic energy $\bar{e} = \frac{1}{2}(\overline{u'^2} + \overline{v'^2} + \overline{w'^2})$ and its vertical component $\overline{w'^2}$ and the temperature variance $\overline{T'^2}$.

We shall only report here rate equations for vertical fluxes and eddy kinetic energy, which read

$$\frac{\partial \overline{u'w'}}{\partial t} = -\frac{\partial}{\partial z}\overline{u'w'^2} - (1 - C_5)\left[\overline{w'^2}\frac{\partial \bar{u}}{\partial z} + \beta\overline{u'T'}\right] - C_4\frac{\bar{e}^{1/2}}{l}\overline{u'w'}, \tag{3}$$

$$\frac{\partial \overline{w'T'}}{\partial t} = -\frac{\partial}{\partial z}\overline{w'^2T'} - \overline{w'^2}\frac{\partial \bar{T}}{\partial z} - (1 - C_7)\beta\overline{T'^2} - C_6\frac{\bar{e}^{1/2}}{l}\overline{w'T'}, \tag{4}$$

$$\frac{\partial \bar{e}}{\partial t} = -\frac{\partial}{\partial z}\overline{w'e} - \overline{u'w'}\frac{\partial \bar{u}}{\partial z} - \beta\overline{w'T'} - \frac{\bar{e}^{3/2}}{l}, \tag{5}$$

where β is the buoyancy parameter and l a mixing length whose values are given in Appendix A together with some explanations concerning the parameterizations used in Eqs. (3)–(5).

The unknown triple-correlation terms appearing in Eqs. (3)–(5), as well as others that are necessary to close the system, are computed by solving their rate equations. We shall only give here the equation for the physically important turbulent vertical flux of eddy kinetic energy

$$\frac{\partial \overline{w'e}}{\partial t} = -\overline{w'^2}\frac{\partial(\bar{e} + \overline{w'^2})}{\partial z} - \overline{u'w'}\frac{\partial \overline{u'w'}}{\partial z} - (1 - C_{11})\left[\overline{u'w'^2}\frac{\partial \bar{u}}{\partial z} + \beta(\overline{eT'} + \overline{w'^2T'})\right] - C_8\frac{\bar{e}^{1/2}}{l}\overline{w'e}. \tag{6}$$

More equations and details are given in Appendix A, together with the rationale used for the parameterizations of various effects.

The model is discretized on a vertical staggered grid with 60 levels and a grid size, $\Delta z = 0.5$ m. The time integration is performed using the Euler-backward scheme with a time step, $\Delta t = 4$ s. Initial and forcing conditions are described in the next section.

The use of a staggered grid makes it possible to introduce boundary conditions at the top of the model, i.e., at the air–sea interface, only for double correlations. Those are taken according to the Monin-Obukhov similarity theory (see André *et al.*, 1978, for more details):

$$\overline{u'w'} = u_*^2; \quad \overline{w'T'} = Q_0; \quad \bar{e} = 3.75u_*^2 + 0.3w_*^2, \tag{7}$$

where w_* is the convective velocity scale (Deardorff, 1970). These boundary conditions, which have been proposed by Wyngaard and Coté (1974), take into account the effect of rolls whose velocity scales with w_*. This choice of fairly simple boundary conditions could appear rather arbitrary. The applicability of Monin-Obukhov similarity theory for the upper part of the OSBL is indeed debated, e.g., see the contradictory arguments by Philipps (1966) and Kraus (1972). Recent findings by Dillon *et al.* (1981), who have shown that the dissipation rate of eddy kinetic energy varies almost logarithmically with depth in the upper part of the OSBL, nevertheless indicate that Monin-Obukhov theory, or at least some of its consequences, may apply for the situation considered here (see also Kitaigorodskii *et al.*, 1983).

It should be emphasized that the model is quite sophisticated as far as turbulence dynamics is con-

cerned, but that it does not include physical phenomena like velocity shearing or internal oscillations due to Coriolis forcing, which have been shown to be of importance, at least within the thermocline (e.g., Krauss, 1981). It neither takes into account pressure diffusion of eddy kinetic energy, which can describe energy fluxes due to gravity waves in the thermocline, nor wave-induced surface energy flux. There is no physical reason for neglecting these fluxes, although it can be noted that they may partially balance each other (Lumley, 1978), or even cancel each other (Caughey and Wyngaard, 1979).

Once again our choice amounts to simplicity in the absence of justified and/or tested parameterization schemes for these processes. This would be a severe limitation if one would use the model to simulate real-world data, but it is believed this is of no real importance as far as one is only interested in special processes, as we are here. This finally further allows for the use of the above simplified boundary conditions.

3. Mean structure corresponding to shear- and/or buoyancy-driven cases

In order to answer the two questions asked in the introduction, the model has been used to simulate three different cases, which are chosen so as to be representative of situations of physical importance. For the three cases the initial conditions are similar: a mixed layer with constant current and temperature down to 7 m, a transition zone with current and temperature jumps, and a deeper ocean at rest ($\bar{u} = 0$) which is stably stratified with a temperature lapse rate γ equal to 4×10^{-2} K m^{-1} (see Figs. 1 and 2).

The first case concerns a stress-driven OSBL with an imposed friction velocity u_* equal to 1 cm s^{-1} and no surface heat flux. The second case refers to wintertime, buoyancy-driven OSBL with an imposed cooling heat flux Q_0 equal to 5×10^{-5} K m s^{-1}, that is roughly 200 W m^{-2}. There is no applied friction velocity and the shear at the bottom of the OSBL remains negligible as in the preceding case. In the third case one tries to simulate a composite case in which cooling is applied from above at the same rate, with no surface stress, but where larger shear at the bottom of the OSBL ($\Delta\bar{u} = 0.1$ m s^{-1} instead of 0.05 m s^{-1} for the first two cases) generates additional turbulence. This additional generation corresponds to friction with the underlying layers, roughly equivalent to a friction velocity equal to 0.15 cm s^{-1}. Since one wants to compare the turbulence structure for these three cases, it is necessary that the interfacial Richardson number

$$\mathrm{Ri} = \frac{\beta \Delta\bar{T} \Delta z}{(\Delta\bar{u})^2}$$

be the same, at least at initial time. We retained for Ri a moderate, close to critical, value, namely Ri = 0.1, leading to a temperature jump $\Delta\bar{T} = 0.25$ K when $\Delta\bar{u} = 5$ cm s^{-1}, i.e. cases (a) and (b), and to $\Delta\bar{T} = 1$ K when $\Delta\bar{u} = 10$ cm s^{-1}, i.e., case (c). Most of the above features are schematically represented in Fig. 1. In the results to be presented below h will be taken as the depth where the temperature variance is a maximum or, equivalently, where the buoyancy flux reaches its maximum positive value.

a. Stress-driven OSBL: Case a

The development of the stress-driven OSBL is shown in Fig. 2a. One can first notice that temperature is progressively redistributed over the depth of the momentum boundary layer. It is further of interest to remark that the efficiency of temperature mixing decreases with depth and that a relatively thick and strong thermocline builds up after a few hours of simulation. The momentum distribution is characterized by an almost constant shear throughout the

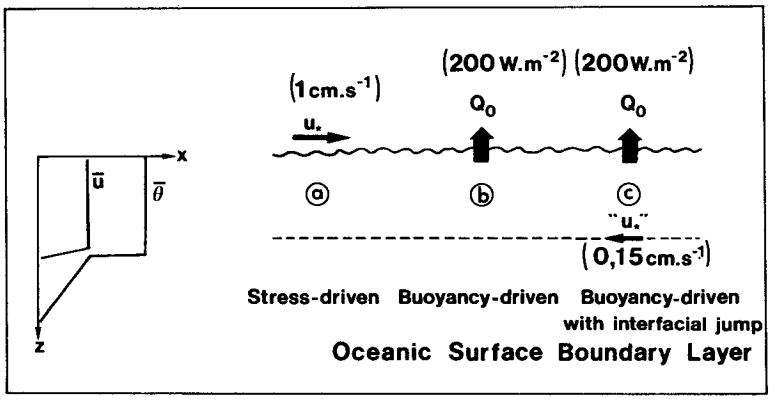

FIG. 1. Schematic representation of the three numerically simulated oceanic surface boundary layers.

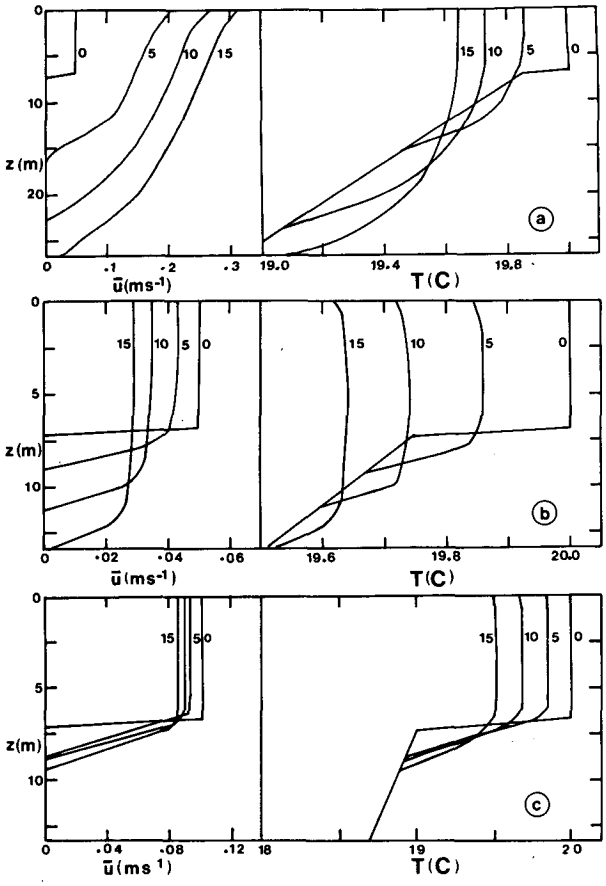

FIG. 2. Vertical profiles of mean current (left) and temperature (right) for three cases depicted in Fig. 1, at initial time and after 5, 10 and 15 h.

whole OSBL depth. This means that the shear-generated turbulence is not efficient enough to mix all the momentum entering through the surface. It is possible to quantify this effect by integrating the momentum equation (1) from the surface to the OSBL bottom

$$\frac{d}{dt}\int_0^h \bar{u}dz = \int_0^h \frac{\partial \bar{u}}{\partial t}\,dz = u_*^2, \tag{8}$$

where it is assumed that both mean velocity and momentum flux vanish at depth h. Since the amount of momentum in the OSBL can be approximated by $\frac{1}{2}hu_s$, where u_s is the surface current, and since the mean shear $\overline{\partial u/\partial z}$ is roughly given by u_s/h, Eq. (8) can be written as

$$\frac{d}{dt}\left(h^2\,\overline{\frac{\partial u}{\partial z}}\right) = 2u_*^2. \tag{9}$$

Development of Eq. (9) using the assumption that mean shear remains almost stationary (see Fig. 2a) leads to

$$\overline{\frac{\partial u}{\partial z}} = \frac{u_s}{h} = \frac{u_*}{h}\left(\frac{dh}{u_* dt}\right)^{-1}. \tag{10}$$

Equation (10) is found to describe quite accurately the numerical results (see Table 1). Equation (10) is very similar to the one that could be obtained by specializing the analysis by André *et al.* (1979b) and Mahrt and André (1983) to the case of a turbulent layer gaining momentum, i.e.,

$$\overline{\frac{\partial u}{\partial z}} = c_u\frac{u_*}{h}. \tag{11}$$

The present analysis indeed shows that the constant c_u appearing in the dimensional relation (11) depends on the deepening rate of the OSBL, i.e., probably on a bulk Richardson number involving the buoyancy variation at the interface with the thermocline. This nondimensional deepening rate varies slightly during the course of the numerical simulation but its value remains between 0.02 and 0.05, i.e. is consistent with a value of approximately 25 for c_u, fairly close to values previously obtained by André *et al.* (1979b) and Mahrt and André (1983) (see Table 1).

b. Buoyancy-driven OSBL: Case b

The development of the buoyancy-driven OSBL is shown in Fig. 2b. First, it is clear that momentum is almost constant throughout the whole layer, in qualitative agreement with the arguments presented above. In this case there is indeed no momentum input at the surface so that convectively generated turbulence may mix momentum efficiently. Also notice that the temperature profiles remain slightly unstable in the upper part of the OSBL and that the transition zone with the deeper thermocline is much thinner than in the preceding case. We shall return to this point in the next section.

TABLE 1. Shear scaling in a stress-driven OSBL ($u_* = 10^{-2}$ m s^{-1}).

Time	h (m)	dh/dt (m s^{-1})	U_s (m s^{-1})	$\overline{\partial u/\partial z} \sim U_s/h$ (s^{-1})	$(dh/u_*dt)^{-1}$	$(u_*/h)(dh/u_*dt)^{-1}$ (s^{-1})	$C_u = (h/u_*)\overline{\partial u/\partial z}$
5 h	13.5	4.8 10^{-4}	0.21	1.55 10^{-2}	20.8	1.54 10^{-2}	21
10 h	20.0	3.3 10^{-4}	0.27	1.34 10^{-2}	30.3	1.51 10^{-2}	27
15 h	24.5	2.0 10^{-4}	0.31	1.24 10^{-2}	50.0	2.04 10^{-2}	30

TABLE 2. Deepening of a buoyancy-driven OSBL.

Time	h (m)	dh/dt (m s^{-1})	$\Delta\bar{T}$ (K)	$W_* = (\alpha g Q_0 h)^{1/3}$ (m s^{-1})	$(dh/w_* dt)^{-1}$	$B_1 = (dh/dt)(\gamma h/Q_0)$	$B_2 = (dh/dt)\left(\frac{\Delta\bar{T}}{Q_0}\right)$
5 h	8	$1.57\ 10^{-4}$	0.185	$9.4\ 10^{-3}$	59.9	1.00	0.58
10 h	10.5	$1.17\ 10^{-4}$	0.145	$1.01\ 10^{-2}$	86.3	0.98	0.34
15 h	12.5	$1.09\ 10^{-4}$	0.127	$1.07\ 10^{-2}$	98.2	1.09	0.28

Table 2 shows that the dimensionless deepening rate now scales with the convective velocity scale w_* (Deardorff, 1970). It also indicates that the numbers $B_i = \Theta dh/Q_0 dt$, where Θ is a temperature scale equal to either γh (product of the underlying lapse rate by the actual depth of the OSBL) or $\Delta\bar{T}$ (interfacial temperature jump) remain within reasonable limits. According to Tennekes (1973), B_1 should be equal to $(1 + 2A)$, where A is the ratio of bottom to surface heat fluxes. This would lead to a value very close to zero for A, much too small as compared to the commonly accepted value of 0.2 (Stull, 1976; Artaz and André, 1980). On the other hand B_2 should be equal to this same number A if the interfacial layer between the OSBL and the underlying layer was infinitely thin. Table 2 indicates that this may become true, but only as time elapses. For shorter times, this ratio is much larger than the commonly accepted value of 0.2, showing possible influence of the initial interfacial velocity jump which can enhance the entrainment buoyancy flux (Zeman, 1975, and Dubosclard, 1980).

c. *Buoyancy-driven OSBL with interfacial shear: Case c*

This case is shown in Fig. 2c where the general structure appears to be quite similar to the one corresponding to case (b), with particular concern to the almost vanishing vertical gradients of velocity and temperature. As for case (b), the "overshoot," or depth of the interfacial zone with the deeper thermocline, is of lesser importance than in the case of a purely stress-driven OSBL.

The OSBL deepening rate is approximately two times smaller than for case b. Since the surface heat flux and the underlying lapse rate are the same for both cases, this indicates that a simple parameterization scheme for convective boundary-layer growth rate such as the one where B_1 is taken as a constant does not perform satisfactorily. On the other hand, the fact that dh/dt is reduced by a factor of ~ 2 when the interfacial Richardson number remains the same, but when the interfacial temperature and velocity jumps are multiplied respectively by 4 and 2, indicates that a proper parameterization scheme for dh/dt must account for

(i) inhibition due to interfacial buoyancy jump, and consequently include $\Delta\bar{T}$ as the temperature scale;

(ii) enhancement of entrainment fluxes due to shear, i.e., allow the number A to be a function of shear.

This last point will be further evidenced in the next section.

4. Turbulence structure and eddy kinetic energy budgets

Many features described in the preceding section can be understood by simply considering turbulence structure or eddy kinetic energy (EKE) budgets. Such budgets correspond to the stationary form of Eq. (5), where the right-hand side includes contributions due to, from left to right, turbulent transfer, shear production, buoyant production and viscous dissipation.

In case (a) of a stress-driven OSBL, the EKE budget has a very simple structure as shown in Fig. 3, taken at $t = 15$ h after the beginning of the experiment. Shear production is a maximum close to the surface, decreasing rapidly to a constant value for most of the rest of the OSBL. It is worth noticing that there is no secondary maximum of EKE production at the bottom of the OSBL, because of the fact that there is no enhanced shear at this level (see Fig. 2a). The budget is furthermore characterized by an equilibrium at each level between shear production and destruction by molecular dissipation and, to a much lesser extent, by conversion into potential energy (see also Simpson and Dickey, 1981, for a similar result obtained with a much simpler turbulence model).

These result in an almost vanishing transfer by turbulence, except immediately beneath the surface and around OSBL bottom, where some EKE is imported respectively from the surface and the interior of the turbulent layer. Figure 6a, also taken at $t = 15$ h, shows that in this case EKE decreases regularly from its surface value equal to $3.75\ u_*^2$ [see Eq. (7)] to zero at $z = h$, explaining why the turbulent EKE flux $w'e$ remains oriented downward. This flux decreases also with increasing depth, the flux divergence being of the order of $0.3\ u_*^3/h$, i.e., less than 10% of the other terms of the budget.

In case (b) of a convectively-driven OSBL, the EKE budget at $t = 15$ h is drastically different (see

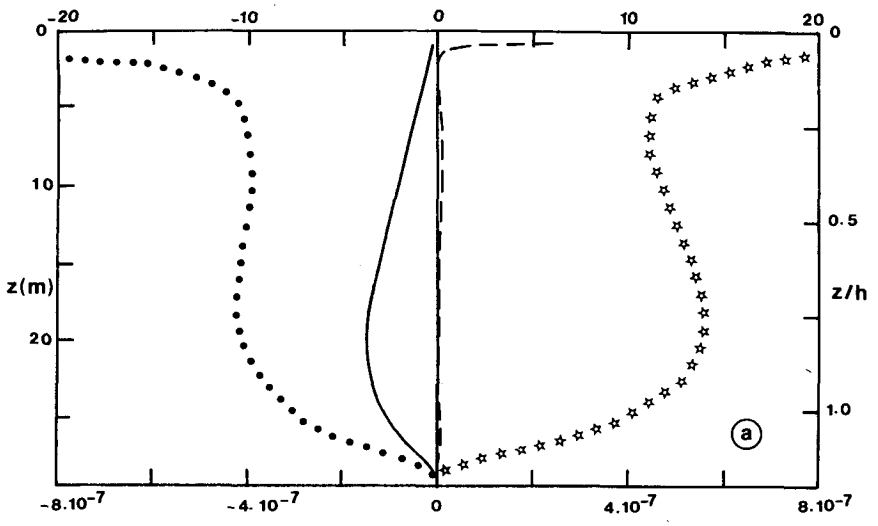

FIG. 3. Eddy kinetic energy budget in the stress-driven case at t = 15 h: buoyant production (solid line), shear production (stars), viscous dissipation (dotted line), turbulent transport (dashed line). The upper units are normalized by u_*^3/h while the lower ones are $m^2 s^{-3}$.

Fig. 4). Buoyant generation is a maximum at the surface and decreases linearly down to the so-called "overshoot" where it reverses sign, indicating a conversion of EKE into potential energy. Shear production remains negligible except around $z = h$, where a momentum jump can be observed (see Fig. 2b). A main qualitative difference with the earlier budget is that now viscous dissipation is not important enough to balance production locally, although the dissipation profile varies qualitatively like the production profile. The excess of EKE production close to the surface corresponds to a downward export to the lower half of the OSBL by turbulent transport. This budget bears very strong resemblances to those already measured in the laboratory (Willis and Deardorff, 1974) and in the atmosphere (e.g., Lenschow, 1974). Vertical velocity variance through which EKE is buoyantly produced [see Eqs. (5) and (A1)], cannot survive easily in the upper part of the OSBL because of the presence of the surface. This explains why in Fig. 6b the EKE profile reaches its maximum within the core of the OSBL, approximately around $z = h/3$. Despite this EKE-distribution, the turbulent flux $w'e$ is not oriented upward in the upper part of the OSBL, but remains almost everywhere oriented downward to the deeper thermocline. It first increases with depth down to $z \sim h/2$, corresponding to the exportation shown in Fig. 4, and then decreases down to zero at $z = h$ in the lower part where EKE is imported. As already suggested, this profile of vertical turbulent flux of

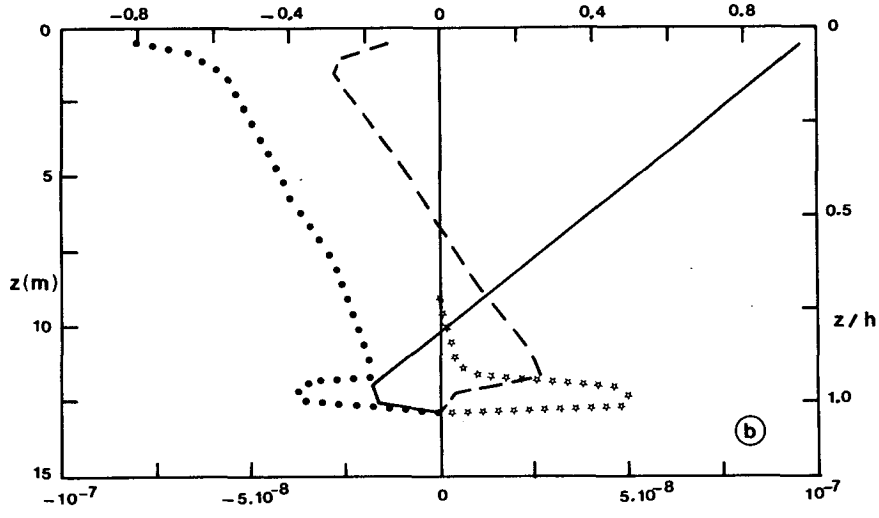

FIG. 4. Eddy kinetic energy budget in the buoyancy-driven case at t = 15 h. Symbols as in Fig. 3, except for the upper units which are normalized by w_*^3/h.

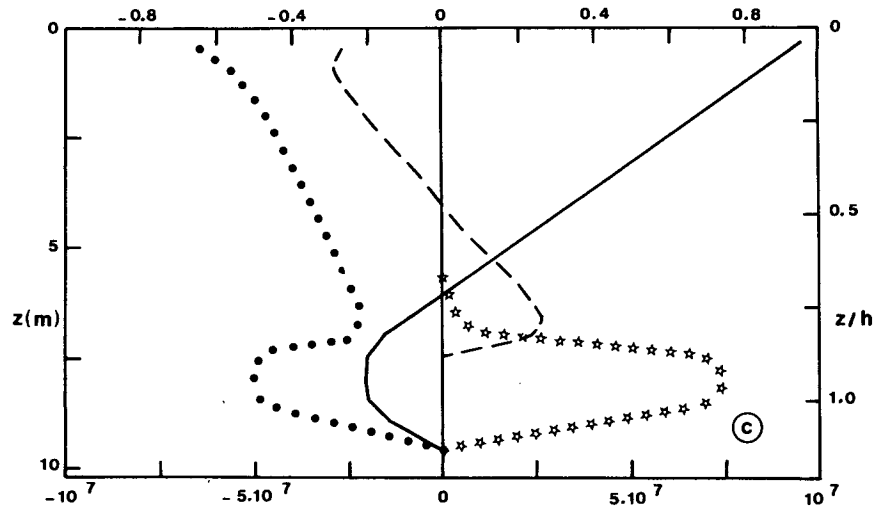

FIG. 5. Eddy kinetic energy budget in the buoyancy-driven case with interfacial jump at t = 15 h. Symbols as in Fig. 4.

EKE cannot be understood by simply considering the EKE distribution.

One has to deal with two different regions in the OSBL: a countergradient diffusion of EKE takes place close to the surface, while gradient diffusion occurs deeper in the OSBL. This feature is well known for convective flows (e.g., see André *et al.*, 1976b, and Zeman and Lumley, 1976) and can now be parameterized in the framework of simple models. Therry and Lacarrère (1983) propose to generalize Deardorff's (1972) analysis of countergradient heat transport to the transport of EKE by including a term proportional to $\overline{w'T'}$ in the parameterization for $\overline{w'e}$. This is intended to account for the buoyant production of EKE, and makes it possible to reproduce the correct sign of the vertical turbulent flux of EKE.

Figure 5 shows the EKE budget at t = 15 h in the intermediate case (c), where approximately the same amount of EKE is generated either buoyantly at the surface or by shear instability at the bottom of the OSBL. First, note that the budget in the upper part of the OSBL is qualitatively similar to the convective one shown in Fig. 4: excess of buoyancy production close to the surface as compared to the local viscous dissipation is associated with a downward export by turbulent transfer to the middle of the OSBL. Second, the budget in the lower part of the OSBL, for $z > 0.75$ h, presents the same general features as the ones corresponding to a stress-driven case, see Fig. 3: local equilibrium between shear production and destruction by either viscous dissipation or conversion into potential energy, with vanishing vertical exchange between layers. A third very interesting feature concerns the thickness and magnitude of the overshoot: as already proposed by Zeman (1975) and observed by Dubosclard (1980) in the atmosphere, the locally shear-induced production of EKE at the edge of the

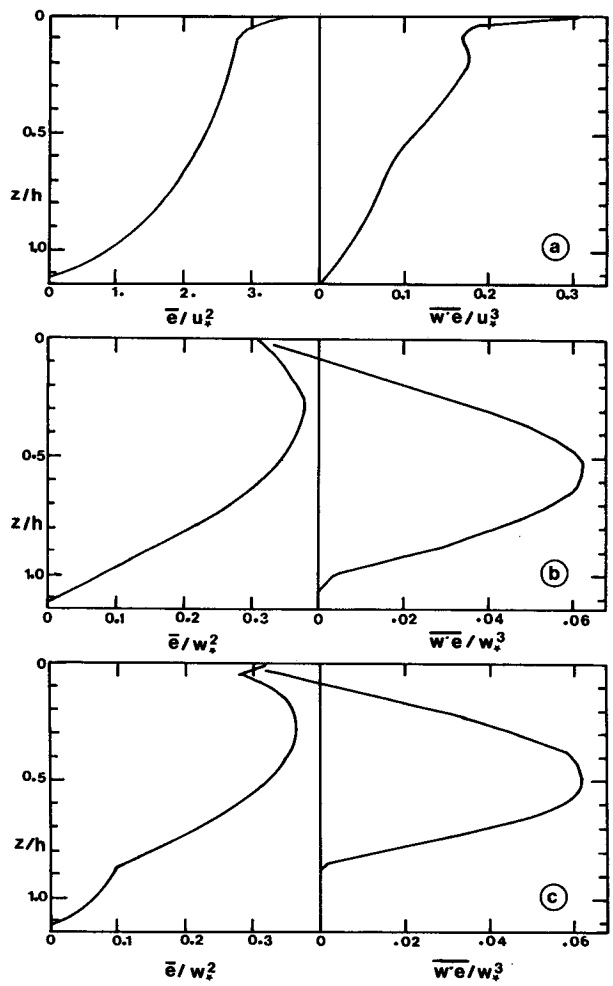

FIG. 6. Normalized profiles of eddy kinetic energy (left) and its turbulent vertical flux (right) at t = 15 h for the three cases depicted in Fig. 1.

thickening boundary layer enhances entrainment of the adjacent stable layer into the mixed layer, and consequently leads to a thinner overshoot and to a larger conversion into potential energy.

Consequences of the above characteristics can be observed in Fig. 6c, taken at $t = 15$ h, where a layer with convective-like distributions of EKE and of its vertical turbulent flux is seen to override, without much interaction, a layer with slightly enhanced EKE but without vertical turbulent transport. The strong shear in the entrainment zone (see Figs. 2c and 5) indeed wipes out the convective transport term there, causing it to approach zero at a height nearer 0.8 h than 1.0 h as in case (b).

Such a local equilibrium between shear production and viscous dissipation has been reported by Crawford and Osborn (1981) in regions where large shear occurs, as is the case in the equatorial part of the Pacific Ocean where the wind-driven South Equatorial Current flows at speeds of 1 to 1.5 m s^{-1} above the Equatorial Undercurrent. Lange (1981) also observed during the MILE experiment maxima of dissipation at the interface between the mixed layer and the thermocline, after a wind event had put the OSBL into motion and consequently created a rather strong interfacial shear. Finally similar situations have also been documented recently in the atmosphere by Brost *et al.* (1982), off the California coast west of San Francisco, in a stratocumulus-topped mixed layer. The layer interior was also neutrally stratified with an intense EKE source at the surface, which however in this case was due to shear instead of convection. Turbulent transport was similarly exporting EKE from this production region to the deeper part of the turbulent layer and did also vanish in the "overshoot," i.e., the transition region with the adjacent stably stratified layer, where a very important shear production was locally balanced by viscous dissipation and conversion into potential energy.

The above numerical and experimental results confirm that the magnitude and vertical distribution of the turbulent flux of EKE is determined not only from the EKE distribution, but also from the nature of the various production mechanisms.

5. Parameterization of the eddy kinetic energy flux

As mentioned in the preceding section, the eddy-kinetic energy model of Therry and Lacarrère (TL) (1983) can be used to describe the turbulent structure of the OSBL. In this model, which is fully presented in Appendix B, the vertical turbulent flux of EKE is computed diagnostically from

$$\overline{w'e} = -0.65\left\{l_K\bar{e}^{1/2}\frac{\partial \bar{e}}{\partial z} + 0.5l\bar{e}^{1/2}\beta w_*\overline{w'T'} + 0.83l\bar{e}^{1/2}\overline{u'w'}\frac{\partial \bar{u}}{\partial z}\right\} \quad (12a)$$

instead of being computed from its rate equation (6) as in the third-order model. In Eq. (12a) the diffusive length l_K is computed from

$$l_K = l\left\{1 - \frac{\beta\overline{w'T'}l}{\bar{e}^{3/2}}\right\}, \quad (12b)$$

where the dissipative length l is the same as in the third-order model, see Eqs. (A4, 5 and 6).

In order to test its ability at reproducing the different regimes of the OSBL, TL's model is used to simulate the intermediate case (c) where buoyancy and shear act simultaneously, but in different regions. The results are shown in Figs. 7a and 8a. It can be seen that the results are very close to the ones from the third-order model, with particular concern to the depth and momentum and stability profiles of the OSBL (Figs. 7a and 2c), and to the sign and magnitude of the vertical turbulent flux of EKE (Figs. 8a and 6c).

It is of interest to assess the importance and contribution of the various countergradient terms. Results obtained by neglecting these terms in the equation for vertical flux of EKE [i.e., by using the classical eddy-diffusivity formulation $\overline{w'e} = -0.65l_K\bar{e}^{1/2}\partial\bar{e}/\partial z$ instead of Eq. (12)], as well as in the heat flux equation [see Eq. (B2) in Appendix B] are shown in Figs. 7b and 8b. By comparing Figs. 7a and 7b it can be seen first that in the absence of countergradient processes the calculated OSBL develops spurious unstable stratification within its upper part driven by convection, in order to support down-

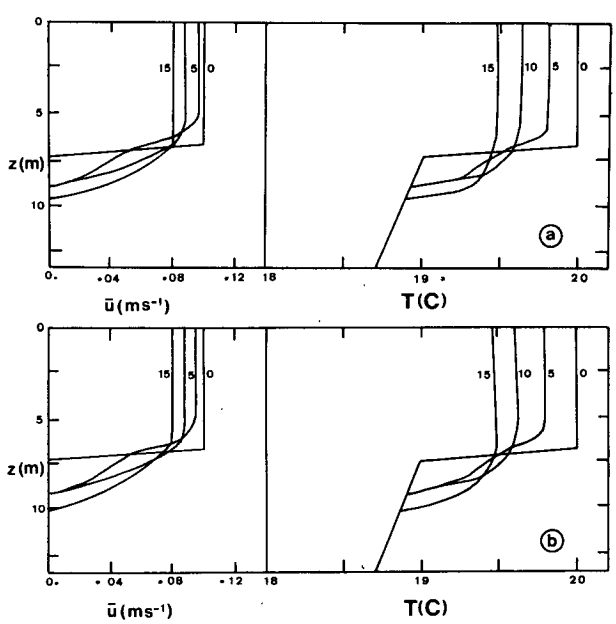

FIG. 7. Vertical profiles of mean current (left) and temperature (right) for case (c) of Fig. 1, using TL eddy kinetic energy model (a) with countergradient diffusion of heat and eddy kinetic energy and (b) without countergradient terms.

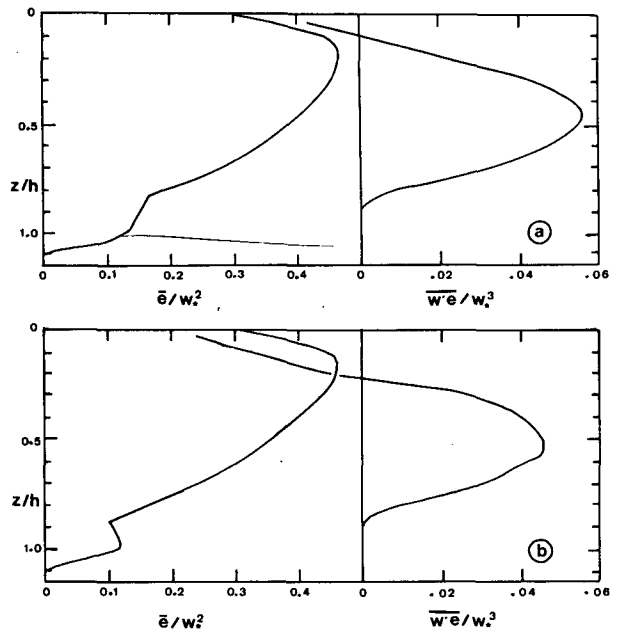

FIG. 8. Normalized profiles of eddy kinetic energy (left) and of its turbulent vertical flux (right) for case (c), using the eddy kinetic energy model (a) with countergradient diffusion of heat and eddy kinetic energy and (b) without countergradient terms.

ward heat fluxes. Second it can be noticed on the same figures that neglecting the countergradient processes leads in this special case to some overestimation of the thickening rate of the OSBL. This last feature can be understood by comparing Figs. 8a and 8b, where it is seen that neglecting countergradient diffusion of EKE leads to reduced downward fluxes of EKE and consequently to an even smaller coupling between the upper buoyancy-driven and the lower shear-driven parts of the OSBL. This in turn amounts to relatively more EKE available for OSBL thickening. It should be emphasized here that an opposite result is found when there is no shear at the bottom of the OSBL, i.e., when neglecting countergradient diffusion leads to an overall underestimation of downward export of EKE, and consequently to an underestimation of OSBL thickening rates.

6. Consequences for turbulence modeling and perspectives

The various cases of oceanic surface boundary layer (OSBL) which have been numerically documented in the present study indicate that it is not always possible to describe the OSBL as a well-mixed layer, as is frequently done in most of the simple parameterized models. This is particularly true for the case of stress-driven OSBL, where a very significant shear survives throughout the whole layer, because of the fact that mechanically induced turbulence is not efficient enough to redistribute the amount of momentum introduced at the surface. On the other hand, turbulence mechanisms in a stress-driven OSBL are fairly simple, since there is not much vertical turbulent coupling, in the sense that eddy kinetic energy (EKE) production is locally balanced by viscous dissipation and buoyancy destruction. In the case of a buoyantly driven OSBL, heat and momentum mixing is much more efficient, which of course leads to a simplified vertical structure, but EKE exchanges are more difficult to parameterize, because of countergradient diffusion. Modeling the entrainment by crudely layer-integrating the turbulence energy budget could then lead to sizeable errors. The relatively simple parameterization by Therry and Lacarrère (1983) has, on the other hand, been shown to lead to a satisfactory description of these countergradient processes.

Even if EKE budget is satisfactorily parameterized from the above point of view, it still remains to account for other processes, which have been neglected in the present study, if one wants to achieve a physically complete description of the real-world OSBL. Among such phenomena, EKE vertical propagation in the thermocline due to internal gravity waves is probably important (e.g., see Kantha, 1977), as well as EKE production due to waves. This last effect is classically known to give rise to an EKE vertical flux at the surface, taken so as to be proportional to the third power of the friction velocity. However, recent experimental studies by Revault d'Allones (1982) in a water-wind tunnel would indicate different behavior. It appears indeed possible that EKE generated by wave-instability in two-dimensional modes could cascade toward larger scales and consequently give rise to structures large enough to erode the thermocline directly. Such a mechanism would probably have to be parameterized using quite different arguments.

Acknowledgments. It is a pleasure to thank J. Deardorff for encouragement and stimulating discussions. Interesting comments and suggestions by P. Bougeault, M. Coantic, B. Cushman-Roisin, T. Dillon, P. Gaspar, E. Kraus and M. Revault d'Allones are gratefully acknowledged.

APPENDIX A

The Third-Order Model

The model used in the present study is basically an upside-down version of the model used for simulations of the atmospheric boundary layer (André *et al.*, 1978; André et Lacarrère, 1980) and of turbulent convection experiments (André *et al.*, 1982).

The rate equations for mean parameters are given by Eqs. (1) and (2). The rate equations for momentum flux $\overline{u'w'}$, heat flux $\overline{w'T'}$ and eddy kinetic energy $\bar{e}$

are given by Eqs. (3) to (5), while the remaining ones for second-order quantities read

$$\frac{\partial \overline{w'^2}}{\partial t} = -\frac{\partial \overline{w'^3}}{\partial z} - 2\left(1 - \frac{2}{3}C_5\right)\beta\overline{w'T'} - \frac{2}{3}C_5\overline{u'w'}\frac{\partial \bar{u}}{\partial z} - C_4\frac{\bar{e}^{1/2}}{l}\left(\overline{w'^2} - \frac{2}{3}\bar{e}\right) - \frac{2}{3}\frac{\bar{e}^{3/2}}{l}, \quad \text{(A1)}$$

$$\frac{\partial \overline{u'T'}}{\partial t} = -\frac{\partial}{\partial z}\overline{u'w'T'} - \overline{u'w'}\frac{\partial \bar{T}}{\partial z} - (1 - C_7)\overline{w'T'}\frac{\partial \bar{u}}{\partial z} - C_6\frac{\bar{e}^{1/2}}{l}\overline{u'T'}, \quad \text{(A2)}$$

$$\frac{\partial \overline{T'^2}}{\partial t} = -\frac{\partial}{\partial z}\overline{w'T'^2} - 2\overline{w'T'}\frac{\partial \bar{T}}{\partial z} - C_2\frac{\bar{e}^{1/2}}{l}\overline{T'^2}. \quad \text{(A3)}$$

The mixing length is chosen as (e.g., see André *et al.*, 1978)

$$l^{-1} = 0.05l_B^{-1} + 0.02[\min(l_B, l_D)]^{-1} \quad \text{(A4)}$$

with l_B being the Blackadar's (1962) length (see Yamada and Mellor, 1975)

$$l_B = \frac{kz}{1 + kz/l_\infty}; \quad k = 0.35; \quad l_\infty = 0.1\frac{\int_0^\infty z\bar{e}^{1/2}dz}{\int_0^\infty \bar{e}^{1/2}dz} \quad \text{(A5)}$$

and l_D the Deardorff (1976) length

$$l_D = 0.075\left[-\bar{e}/\beta\frac{\partial \bar{T}}{\partial z}\right]^{1/2}. \quad \text{(A6)}$$

The Deardorff length defined by Eq. (A6) is proportional to the Ozmidov scale $L_0 = [\epsilon/(-\beta\partial\bar{T}/\partial z)^3]^{1/2}$, which has indeed been shown by Dillon (1982) to be of the same order as the Thorpe scale, i.e., to correctly describe turbulence events in a stably stratified OSBL.

In Eqs. (3) to (5) and (A1) to (A3), the C_4-, C_6-, and C_5-, C_7-terms refer respectively to the parameterization of nonlinear and rapid pressure effects (Launder, 1975) while the C_2-term accounts for the molecular destruction of temperature variance.

The unknown triple terms appearing in Eqs. (3) to (5) and (A1) to (A3) as well as others which are necessary to close the systems, are computed by solving their rate equations, i.e.,

$$\frac{\partial}{\partial t}\overline{u'w'^2} = -\overline{u'w'}\frac{\partial \overline{w'^2}}{\partial z} - 2\overline{w'^2}\frac{\partial \overline{u'w'}}{\partial z} - (1 - C_{11})\times\left\{\overline{w'^3}\frac{\partial \bar{u}}{\partial z} + 2\beta\overline{u'w'T'}\right\} - C_8\frac{\bar{e}^{1/2}}{l}\overline{u'w'^2}, \quad \text{(A7)}$$

$$\frac{\partial}{\partial t}\overline{w'^2T'} = -\overline{w'T'}\frac{\partial \overline{w'^2}}{\partial z} - 2\overline{w'^2}\frac{\partial \overline{w'T'}}{\partial z} - \overline{w'^3}\frac{\partial \bar{T}}{\partial z} - 2\left(1 - \frac{2}{3}C_{11}\right)\beta\overline{w'T'^2} - \frac{2}{3}C_{11}\overline{u'w'T'}\frac{\partial \bar{u}}{\partial z} - C_8\frac{\bar{e}^{1/2}}{l}\overline{w'^2T'}, \quad \text{(A8)}$$

$$\frac{\partial}{\partial t}\overline{w'^3} = -3\overline{w'^2}\frac{\partial \overline{w'^2}}{\partial z} - 3(1 - C_{11})\beta\overline{w'^2T'} - C_8\frac{\bar{e}^{1/2}}{l}\overline{w'^3}, \quad \text{(A9)}$$

$$\frac{\partial}{\partial t}\overline{u'w'T'} = -\overline{w'T'}\frac{\partial \overline{u'w'}}{\partial z} - \overline{w'^2}\frac{\partial \overline{u'T'}}{\partial z} - \overline{u'w'}\frac{\partial \overline{w'T'}}{\partial z} - \overline{u'w'^2}\frac{\partial \bar{T}}{\partial z} - (1 - C_{11})\times\left\{\overline{w'^2T'}\frac{\partial \bar{u}}{\partial z} + \beta\overline{u'T'^2}\right\} - C_8\frac{\bar{e}^{1/2}}{l}\overline{u'w'T'}, \quad \text{(A10)}$$

$$\frac{\partial}{\partial t}\overline{w'T'^2} = -2\overline{w'T'}\frac{\partial \overline{w'T'}}{\partial z} - \overline{w'^2}\frac{\partial \overline{T'^2}}{\partial z} - 2\overline{w'^2T'}\frac{\partial \bar{T}}{\partial z} - (1 - C_{11})\beta\overline{T'^3} - C_8\frac{\bar{e}^{1/2}}{l}\overline{w'T'^2}, \quad \text{(A11)}$$

$$\frac{\partial}{\partial t}\overline{eT'} = -\overline{w'T'}\frac{\partial \bar{e}}{\partial z} - \overline{w'^2}\frac{\partial \overline{w'T'}}{\partial z} - \overline{u'w'}\frac{\partial \overline{u'T'}}{\partial z} - \overline{u'w'T'}\frac{\partial \bar{u}}{\partial z} - \overline{w'e}\frac{\partial \bar{T}}{\partial z} - \beta\overline{w'T'^2} - C_8\frac{\bar{e}^{1/2}}{l}\overline{eT'}, \quad \text{(A12)}$$

$$\frac{\partial}{\partial t}\overline{u'T'^2} = -2\overline{w'T'}\frac{\partial \overline{u'T'}}{\partial z} - \overline{u'w'}\frac{\partial \overline{T'^2}}{\partial z} - 2\overline{u'w'T'}\frac{\partial \bar{T}}{\partial z} - (1 - C_{11})\overline{w'T'^2}\frac{\partial \bar{u}}{\partial z} - C_8\frac{\bar{e}^{1/2}}{l}\overline{u'T'^2}, \quad \text{(A13)}$$

$$\frac{\partial}{\partial t}\overline{T'^3} = -3\overline{w'T'}\frac{\partial \overline{T'^2}}{\partial z} - 3\overline{w'T'^2}\frac{\partial \bar{T}}{\partial z} - C_{10}\frac{\bar{e}^{1/2}}{l}\overline{T'^3}. \quad \text{(A14)}$$

In Eqs. (6) and (A7)–(A14) the C_{11} terms are parameterizations of rapid pressure effects while the C_8- and C_{10}- terms account for nonlinear pressure effects and molecular destruction (André *et al.*, 1982). The quasinormal assumption has been used to relate fourth-order moments to second-order ones in Eqs. (6) and (A7) to (A14).

The values of the dimensionless constants used for the parameterization of pressure and molecular effects are as follows:

$$C_2 = 2.5, \quad C_4 = 4.5, \quad C_5 = 0, \quad C_6 = 4.85,$$
$$C_7 = 0.4, \quad C_8 = 8, \quad C_{10} = 7.5, \quad C_{11} = 0.2.$$

The coefficient of thermal expansion α, used to compute the buoyancy parameter $\beta = \alpha g$, is taken as a constant, $\alpha = 2 \times 10^{-4}$ K^{-1}, corresponding to a temperature of approximately 20°C.

The clipping approximation, i.e., the enforcement of realizability inequalities for triple moments in order to prevent unphysical development of negative variances and correlation coefficients greater than one (André *et al.*, 1976a), is used in the present simulations. Its use could be avoided only for the study of the quasi-stationary convective regime in case (b), when improved parameterizations of various effects in the rate equations for triple moments prevent from violation of realizability constraints (see also André, 1984).

APPENDIX B

The Eddy-Kinetic Energy Model

The model used in the present study is basically an upside-down version of the Therry and Lacarrère (1983) model.

The rate equations for mean parameters are given by Eqs. (1) and (2). The rate equation for eddy kinetic energy (EKE) $\bar{e}$ is still given by Eq. (5). The vertical turbulent flux of EKE is computed from Eq. (12a) and the eddy fluxes for momentum and heat are given respectively by

$$\overline{u'w'} = -K_u \frac{\partial \bar{u}}{\partial z}, \tag{B1}$$

$$\overline{w'T'} = -K_\theta \left(\frac{\partial \bar{T}}{\partial z} - \frac{5Q_0}{w_* h} \right), \tag{B2}$$

where

$$K_u = K_\theta = 0.5 l_K \bar{e}^{1/2} \tag{B3}$$

and where l_K is computed from Eq. (12b) and l from Eqs. (A4) to (A6).

REFERENCES

André, J. C., 1984: Comments on atmospheric modelling. *Mech. Eng. Trans.*, (in press).

——, and P. Lacarrère, 1980: Simulation numérique détaillée de la couche limite atmosphérique. Comparison avec la situation des 2 et 3 Juillet 1977 à Voves. *La Météorologie VI*, **22**, 5–49.

——, G. De Moor, P. Lacarrère and R. du Vachat, 1976a: Turbulence approximation for inhomogeneous flows. Part I: The clipping approximation. *J. Atmos. Sci.*, **33**, 476–481.

——, ——, —— and ——, 1976b: Turbulence approximation for inhomogeneous flows. Part II: The numerical simulation of a penetrative convection experiment. *J. Atmos. Sci.*, **33**, 482–491.

——, G. De Moor, P. Lacarrère, G. Therry and R. du Vachat, 1978: Modeling the 24-hour evolution of the mean and turbulent structures of the planetary boundary layer. *J. Atmos. Sci.*, **35**, 1861–1883.

——, P. Lacarrère and L. J. Mahrt, 1979a: Sur la distribution verticale de l'humidité dans une couche limite convective. *J. Rech. Atmos.*, **13**, 135–146.

——, G. De Moor, P. Lacarrère, G. Therry and R. du Vachat, 1979b: The clipping approximation and inhomogeneous turbulence simulations. *Turbulent Shear Flows 1*, Springer-Verlag, 307–318.

——, P. Lacarrère, and K. Traoré, 1982: Pressure effects on triple correlations in turbulent convective flows. *Turbulent Shear Flows 3*, Springer-Verlag, 243–252.

Artaz, M. A., and J. C. André, 1980: Similarity studies of entrainment in convective boundary layers. *Bound.-Layer Meteor.*, **19**, 51–66.

Blackadar, A. K., 1962: The vertical distribution of wind and turbulent exchange in a neutral atmosphere. *J. Geophys. Res.*, **67**, 3095–3102.

Brost, R. A., J. C. Wyngaard and D. H. Lenschow, 1982: Marine stratocumulus layers. Part II: Turbulence budgets. *J. Atmos. Sci.*, **39**, 818–836.

Caughey, J. C., and J. C. Wyngaard,1979: The turbulence kinetic energy budget in convective conditions. *Quart. J. Roy. Meteor. Soc.*, **105**, 221–239.

Chouchan, D., 1981: "Etude de quelques mécanismes d'interaction rapide entre l'atmosphère et l'océan". Thèse 3eme cycle, University de Paris 6.

Crawford, W. R., and T. R. Osborn, 1981: Control of equatorial ocean currents by turbulent dissipation. *Science*, **212**, 539–540.

Cushman-Roisin, B., 1982: Penetrative convection in the upper ocean due to surface cooling. *Geophys. Astrophys. Fluid. Dyn.*, **19**, 61–91.

Deardorff, J. W., 1970: Convective velocity and temperature scales for the unstable boundary layer and for Rayleigh convection. *J. Atmos. Sci.*, **27**, 1211–1213.

——, 1972: Theoretical expression for the countergradient vertical heat flux. *J. Geophys. Res.*, **30**, 5900–5904.

——, 1976: Clear and cloud-capped mixed layers. Their numerical simulation, structure and growth and parameterization. *Seminars on "The treatment of the boundary layer in numerical weather prediction"*, European Center for Medium Range Weather Forecast, Reading, 234–284.

——, 1980: Comments on "A numerical investigation of mixed-layer dynamics". *J. Phys. Oceanogr.*, **10**, 1695–1696.

Denman, K. L., and M. Miyake, 1973: Upper layer modification at ocean station PAPA: Observations and simulation. *J. Phys. Oceanogr.*, **3**, 185–196.

Dillon, T. M., 1982: Vertical overturns: A comparison of Thorpe and Ozmidov length scales. *J. Geophys. Res.*, **87C**, 9601–9613.

——, J. G. Richman, C. G. Hansen and M. D. Pearson, 1981: Near-surface turbulence measurements in a lake. *Nature*, **290**, 390–392.

Dubosclard, G., 1980: A comparison between observed and predicted values for the entrainment coefficient in the planetary boundary layer. *Bound.-Layer Meteor.*, **18**, 473–483.

Garwood, R. W. Jr., 1977: An oceanic mixed layer model capable of simulating cyclic states. *J. Phys. Oceanogr.*, **7**, 455–468.

Gaspar, P., 1984: Modelling the seasonal response of the oceanic mixed layer. *J. Phys. Oceanogr.* (Submitted.)

Kantha, L. H., 1977: Note on the role of internal waves in thermocline erosion. *Modelling and Prediction of the Upper Layer of the Ocean*, E. B. Kraus Ed., Pergamon, 173–177.

Kitaigorodskii, S. A., M. A. Donelan, J. L. Lumley and E. A. Terray, 1983: Wave-turbulence interactions in the upper ocean. Part II: Statistical characteristics of wave and turbulent components of the random velocity field in the marine surface layers. *J. Phys. Oceanogr.*, **13**, 1988–1999.

Klein, P., and M. Coantic, 1981: A numerical study of turbulent processes in the marine upper layers. *J. Phys. Oceanogr.*, **11**, 849–863.

Kraus, E. B., 1972: *Atmosphere-Ocean Interaction.* Oxford University Press, 188–199.

——, and J. S. Turner, 1967: A one-dimensional model of the seasonal thermocline. Part II: The general theory and its consequences. *Tellus,* **19,** 98–106.

Krauss, W., 1981: The erosion of a thermocline. *J. Phys. Oceanogr.,* **11,** 415–433.

Kundu, P. K., 1980a: A numerical investigation of mixed layer dynamics. *J. Phys. Oceanogr.,* **10,** 220–236.

——, 1980b: Reply (to J. W. Deardorff's comment). *J. Phys. Oceanogr.,* **10,** 1697.

——, 1981: Self-similarity in stress-driven entrainment experiments. *J. Geophys. Res.,* **8603,** 1979–1988.

Lacombe, H., 1974: Modèles simples de prévision de l'état thermique de la mer et de l'immersion de la thermocline. *Ann. Hydrog. 5,* **741,** 3–21.

Lange, R. E., 1981: Observations of near-surface oceanic velocity strain-rate variability during and after storm events. *J. Phys. Oceanogr.,* **11,** 1272–1279.

Launder, B. E., 1975: On the effects of a gravitational field on the turbulent transport of heat and momentum. *J. Fluid Mech.,* **67,** 569–581.

Lenschow, D. H., 1974: Model of the height variation of the turbulence kinetic energy budget in the unstable planetary boundary layer. *J. Atmos. Sci.,* **31,** 465–474.

Lumley, J. L., 1978: Computational modelling of turbulent flows. *Advances in Applied Mechanics,* Vol. 18, Academic Press, 123–176.

Mahrt, L., and J. C. André, 1983: On the stratification of turbulent mixed layers. *J. Geophys. Res.,* **88C4,** 2662–2666.

Mellor, G. L., and P. A. Durbin, 1975: The structure and dynamics of the ocean surface mixed layer. *J. Phys. Oceanogr.,* **5,** 718–728.

——, and P. T. Strub, 1980: Similarity solutions for the stratified turbulent Rayleigh problem. *J. Phys. Oceanogr.,* **10,** 455–460.

Phillips, O. M., 1966: *The Dynamics of the Upper Ocean,* Cambridge University Press, 281–308.

Posmentier, E. S., 1980: A numerical study of the effects of heat diffusion through the base of the mixed layer. *J. Geophys. Res.,* **85C9,** 4883–4887.

Price, J. F., R. A. Weller and R. Pinkel, 1984: Diurnal cycling-Observations and models of the upper ocean response to diurnal heating, cooling and wind mixing. *J. Phys. Oceanogr.* (Submitted.)

Revault d'Allones, M., 1982: Une hypothèse sur la structure de la turbulence induite dans l'eau par des vagues fortement cambrées. *C. R. Acad. Sci. Paris.,* **295,** 201–204.

Simpson, J. J., and T. D. Dickey, 1981: The relationship between downward irradiance and upper ocean structure. *J. Phys. Oceanogr.,* **11,** 309–323.

Stull, R., 1976: The energetics of entrainment across a density interface. *J. Atmos. Sci.,* **33,** 1260–1267.

Svensson, U., 1979: The structure of the turbulent Ekman layer. *Tellus,* **31,** 340–350.

Tennekes, H., 1973: A model for the dynamics of the inversion above a convective boundary layer. *J. Atmos. Sci.,* **30,** 558–567.

Therry, G., and P. Lacarrère, 1983: Improving the eddy-kinetic-energy model for planetary boundary-layer description. *Bound.-Layer Meteor.,* **25,** 63–88.

Thompson, R. O. R. Y., 1976: Climatological numerical models of the surface mixed layer of the ocean. *J. Phys. Oceanogr.,* **6,** 496–503.

Warn-Varnas, A. C., and S. A. Piacsek, 1979: "An investigation of the importance of third-order correlations and choice of length scale in mixed layer modelling. *Geophys. Astrophys. Fluid Dyn.,* **13,** 225–243.

Willis, G. E., and J. W. Deardorff, 1974: A laboratory model of the unstable planetary boundary layer. *J. Atmos. Sci.,* **31,** 1297–1307.

Wyngaard, J. C., and O. R. Coté, 1974: The evolution of a convective planetary boundary layer. A higher-order-closure model study. *Bound.-Layer Meteor.,* **7,** 289–308.

Yamada, T., and G. L. Mellor, 1975: A simulation of the Wangara atmospheric boundary layer data. *J. Atmos. Sci.,* **32,** 2309–2329.

Zeman, O., 1975: The dynamics of entrainment in planetary boundary layers: A study in turbulence modeling and parameterization. Ph.D. thesis, Pennsylvania State University.

Zeman, O., and J. L. Lumley, 1976: Modeling buoyancy driven mixed layers. *J. Atmos. Sci.,* **33,** 1974–1988.